Preparation of TiO_2 layers on cp-Ti and Ti6Al4V by thermal and anodic oxidation and by sol-gel coating techniques and their characterization

D. Velten,[1] V. Biehl,[1] F. Aubertin,[1] B. Valeske,[2] W. Possart,[2] J. Breme[1]
[1]*Lehrstuhl für Metallische Werkstoffe, Universität des Saarlandes, Saarbrücken, Germany*
[2]*Lehrstuhl für Polymere und Thermodynamik der Werkstoffe, Universität des Saarlandes, Saarbrücken, Germany*

Received 13 July 2000; accepted 10 May 2001

Abstract: The excellent biocompatibility of titanium and its alloys used, for example, for medical devices, is associated with the properties of their surface oxide. For a better understanding of the tissue reaction in contact with the oxide layer, knowledge of the chemical and physical properties of this layer is of increasing interest. In this study, titania films were produced on cp-Ti and Ti6Al4V substrates by thermal oxidation, anodic oxidation, and by the sol-gel process. The thickness and structure of the films produced under different conditions were determined by ellipsometry, infrared spectroscopy, and X-ray diffraction measurements. The corrosion properties of these layers were investigated by current density–potential curves under physiological conditions. The oxide layers produced on cp-Ti and Ti6Al4V by thermal oxidation consist of TiO_2 in the rutile structure. For the anodized samples the structure of TiO_2 is a mixture of amorphous phase and anatase. The structure of the coatings produced by the sol-gel process for a constant annealing time depends on the annealing temperature, and with increasing temperature successively amorphous, anatase, and rutile structure is observed. Compared to the uncoated, polished substrate with a natural oxide layer, the corrosion resistance of cp-Ti and Ti6Al4V is increased for the samples with an oxide layer thickness of about 100 nm, independent of the oxidation procedure. © 2001 John Wiley & Sons, Inc. J Biomed Mater Res 59: 18–28, 2002

Key words: titanium oxide layer; thermal oxidation; anodic oxidation; sol-gel process; corrosion resistance

INTRODUCTION

In the past 20 years titanium and its alloys have gained more and more attraction as materials for surgical applications because of their prominent mechanical, chemical, and biocompatible properties.[1–3] The excellent biocompatibility is achieved by a dense TiO_2 layer that is always present in oxidizing media as in the human body fluid, and is rebuilt within milliseconds after any damaging.[4] As a result, the tissue around a surgical implant is in contact with the surface oxide layer and not with the metal itself. As titanium and titanium alloys used for biomedical application are always covered with a dense oxide film, the properties of the film determine the corrosion behavior of the metal or alloy. It is of interest to investigate the influence of the film structure, composition, and thickness on the corrosion behavior and on the biocompatibility. Therefore, knowledge of the chemical and physical properties of titanium oxide layers on titanium and titanium alloys is important for the reaction of cells in contact with biomaterials made of titanium and titanium alloys.

To improve the integration process of surgical implants in the human body, components of surrounding tissue, for example, collagen or proteins, are immobilized at the oxide layer of the implant. The preparation of titanium oxide layers with a known structure and thickness as an initial state for this biologization procedure is of growing interest.[3] This shows the need for well-defined titanium oxide films and how they can be modified and tailored.

Due to its high affinity to oxygen, titanium forms several oxides in various crystal modifications. In normal atmosphere the thermodynamically stable oxide is TiO_2, which exists in three allotropic modifications: (1) Rutile, (2) Brookite, and (3) Anatase.

Table I gives the structure and some physical properties of these TiO_2 modifications.[8–10] Rutile is thermodynamically the most stable modification[6] and has the highest dielectric constant of $\varepsilon = 110$, which is inde-

Correspondence to: D. Velten; e-mail: d.velten@mx.uni-saarland.de

Contract grant sponsor: Deutsche Forschungsgemeinschaft

TABLE I
Crystal Structure and Some Physical Properties of the Three TiO_2 Modifications

	Rutile	Brookite	Anatase
Elementary cell	Tetragonal	Orthorhombic	Tetragonal
Atomic distance [Å]	a = 4.5937 c = 2.9619	a = 9.185 b = 5.447 c = 5.143	a = 3.785 c = 9.514
Density (g/cm^3)	4.245	4.119	3.893
Molar volume (cm^3/mol)	18.817	19.393	20.519
Heat of formation ΔH^0_{298} (kJ/mol)	945	942	939
Dielectric constant ε	110	78	48

pendent of the frequency up to the GHz region.[1,7] Thin films of TiO_2 can be produced by established processes such as thermal oxidation, anodization, PVD, CVD, plasma spraying, or the sol-gel process.[11–19]

In this study, TiO_2 layers on cp-Ti and Ti6Al4V were produced by thermal and anodic oxidation and by the sol-gel technique as a coating procedure. The aim was the determination of the influence of such production parameters as time and temperature, in the case of the thermal oxidation, polarization current density, and polarization voltage, in the case of the anodic oxidation, on the structure, chemical composition, and thickness of the resulting oxide layers. The sol-gel process has already become a well-established coating technique for the production of TiO_2 layers, especially for coating of glasses.[5]

MATERIALS AND METHODS

Production of the oxide layers

For the determination of the influence of the coating and oxidizing parameters on the structure and thickness of the TiO_2 layers, plates of commercially pure Titanium (cp-Ti, grade II) and Ti6Al4V were used (20 mm diameter, 5 mm thickness). To achieve reproducible surfaces, all samples were mechanically ground with SiC and mechanically polished with a mixture of SiO_2 suspension, distilled water, and H_2O_2. After cleaning and drying, the surface quality of the samples was inspected with a light microscope (polarized light). Figure 1 shows the surface of cp-Ti and Ti6Al4V samples after the described preparation. An equiaxed microstructure consisting of α-phase (cp-Ti) and a fine-grained (α + β) microstructure (Ti6Al4V) without preparation marks are visible. Because of their different orientation the α-phase grains show different gray colors.

Thermal oxidation of the samples was performed in a laboratory furnace in atmosphere at temperatures between 400 and 600°C for 5–500 min.

Anodic oxidation was performed in 0.5 molar H_2SO_4 at room temperature (Fig. 2). A thin wire consisting of cp-Ti was spot welded to the samples to connect them as an anode in an galvanostatic circuit. A Pt-electrode was used as the counter electrode. Oxygen was permanently bubbled through the electrolyte to achieve a constant concentration during the process. During the oxidation, the current density was adjusted by an galvanostat resulting in a permanently increasing potential. When the desired final potential was reached the power supply was immediately switched off. The final potentials at which the power supply was switched off ranged from 7.5 to 100 V. For cp-Ti the applied constant current density was 5 mA/cm^2 for final potentials from 7.5 to 50 V and 10 mA/cm^2 for 50 to 100 V. For Ti6Al4V, the current density was 2 mA/cm^2 for the range of potential up to 100 V.

The oxide layers produced by thermal or anodic oxidation are built up by the reaction of the substrate material with the surrounding oxygen or electrolyte. Thus, the oxide film of the alloy may contain, besides Ti and O, other elements such as Al or V. By contrast, with the sol-gel process it is possible to produce pure TiO_2 layers.

For the sol-gel process mixtures of a metal alkoxide (tetra-*n*-butyl orthotitanate TBOT, $Ti(OC_4H_9)_4$) and a solvent (ethanol, C_2H_5OH) have been used (3 mol % TBOT + 97 mol % ethanol, 1 mol % TBOT + 99 mol % ethanol). Chemical additives that may include stabilizing agents were not used because of a possible negative influence on the biocompatibility of the films. With this sol the samples are spin coated (6000 rpm).

Because of the large surface area of the coated sample, the solvent of the sol evaporates and at the same time the alkoxide is hydrolyzed by the atmospheric water, forming titanium hydroxide and butanol according to (1):

$$Ti(OC_4H_9)_4 + 4 \cdot H_2O \rightarrow Ti(OH)_4 + 4 \cdot C_4H_9OH \quad (1)$$

During ongoing hydrolysis, a polycondensation of the hydrolyzed particles occurs, with the $Ti(OH)_4$ molecules form-

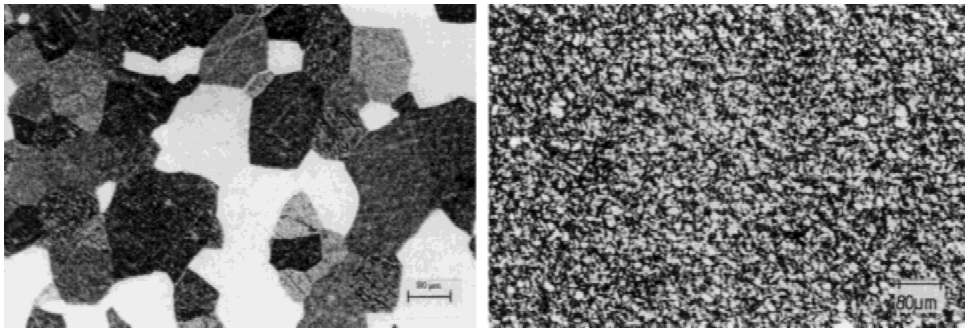

Figure 1. Polished surface of cp-Ti (left) and Ti6A14V (right), bar = 80 μm.

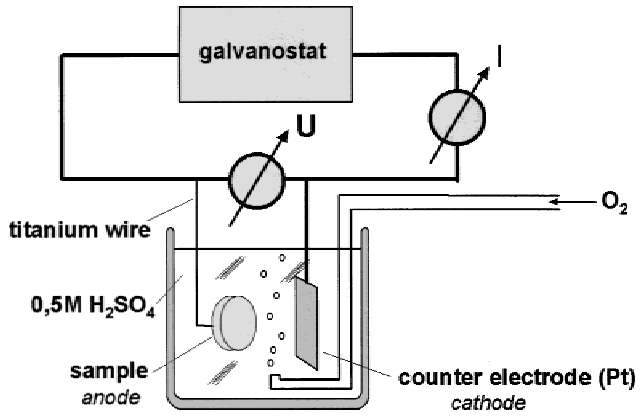

Figure 2. Experimental setup for anodic oxidation.

ing –Ti–O–Ti– connections by elimination of water according (2):

$$2 \cdot Ti(OH)_4 \rightarrow (OH)_3Ti\text{–}O\text{–}Ti(OH)_3 + H_2O \qquad (2)$$

When this reaction is repeated, nanometer sized, amorphous TiO_2 particles consisting of a three dimensional network of —Ti—O—Ti— connections, are formed.

After the coating process, the samples are dried in a furnace at 130°C for 30 min. During this drying, most of the ethanol, butanol, and water evaporate, resulting in an agglomeration of the TiO_2 particles in the film (gel formation). If thicker layers are required, coating with subsequent drying is repeated several times. In the final annealing process at temperatures between 300 and 750°C for 1 h, residual organic components are removed. At the same time, crystallization and solidification of the TiO_2 layer takes place. Figure 3 shows schematically the reactions occurring during the sol-gel coating process.

Characterization techniques

Depending on the conditions of production, most of the TiO_2 layers are transparent in the VIS range up to a thickness of about 300 nm. The thickness of the films was determined by means of a variable angle spectroscopic ellipsometer (VASE, Woollam) and the structure of the oxide layers by means of FTIR spectrometry (IFS 66 v/s, Bruker) in the reflection mode (70°, *p*-polarized light). For reference, spectra of polished cp-Ti and Ti6Al4V with a thin natural oxide layer were used.

The influence of the crystallization temperature on the structure of the oxide produced by the sol-gel process was measured with XRD. As the oxide layers are too thin for direct detection, titania powder was produced by concentrating the sol. Following this, the powder was heat treated

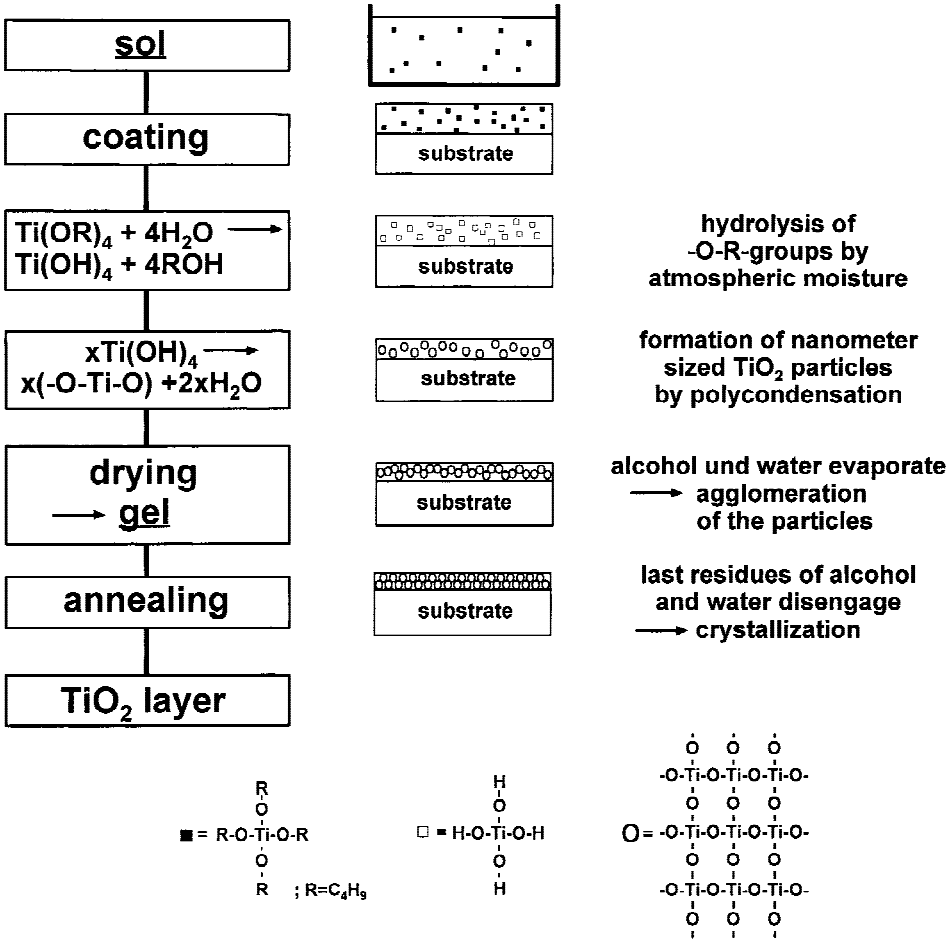

Figure 3. Schematic description of sol-gel chemistry.

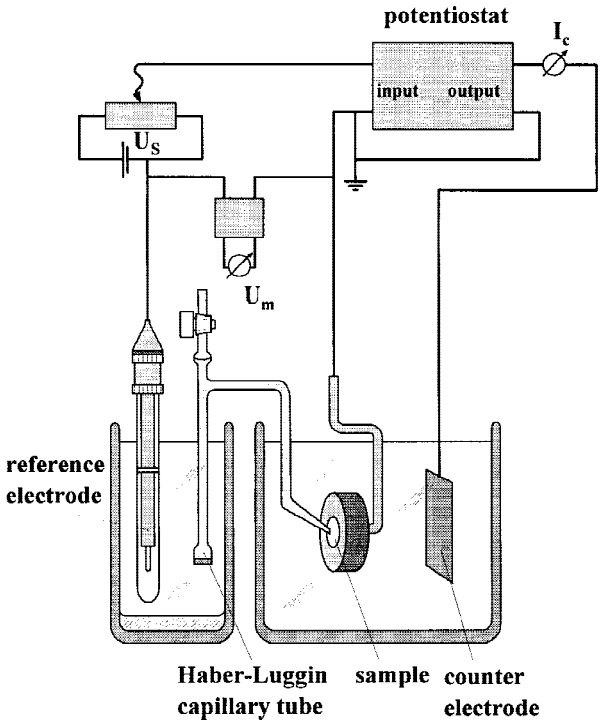

Figure 4. Experimental setup for the determination of current density–potential curves.

at different temperatures and XRD patterns were measured. The identification of the peaks was made with spectra of reference samples (commercial anatase and rutile powders). The influence of various oxide layers on titanium and titanium alloys on the corrosion properties, which are caused by the ion and electron transport through the oxide layer, was determined by measuring current density–potential curves under physiological conditions (37°C, 0.9 % NaCl in H_2O, saturated with oxygen).

The current density–potential curves were determined with the experimental setup shown in Figure 4. The potential, applied between the working (sample) and the reference electrode (Argenthal Ag/AgCl, +207 mV to NHE), was varied from −1000 to +3000 mV at a scan rate of 0.5 mV/s. For a better determination of the current density in the range of passivity the scan rate was decreased to 0.1 mV/s in separate tests.

TABLE II
Colors of Oxide Layers after Thermal Oxidation

Layer Thickness (nm)	10–25	25–40	40–50	50–80
Color	golden	purple	deep blue	light blue

RESULTS AND DISCUSSION

Coatings produced by means of the thermal oxidation

For cp-Ti, Figure 5 shows the thickness of the oxide layers as a function of time and temperature. As expected, the growth rate increases with increasing temperature. Up to 500°C a logarithmic and at 600°C a parabolic growth rate was observed.

Depending on the layer thickness, different interference colors of the films are visible. Table II gives a description of characteristic colors for different ranges of thickness of the oxide layers. Above 80 nm thickness no relationship between color and thickness can be observed. This is due to the nonuniform oxidation of the differently orientated α-phase grains.

For Ti6Al4V, the growth of the thermal oxide layers is described by a logarithmic law up to 550°C and by a parabolic law for 600°C, as shown in Figure 6. Because of the fine-grained microstructure the samples show a smoother surface and the same colors, but paler than those of cp-Ti.

Infrared spectroscopy was used to determine the structure of the oxide layers after thermal oxidation. Figure 7 shows the reflection spectra of oxide films on cp-Ti and Ti6Al4V with a thickness of about 190 nm.

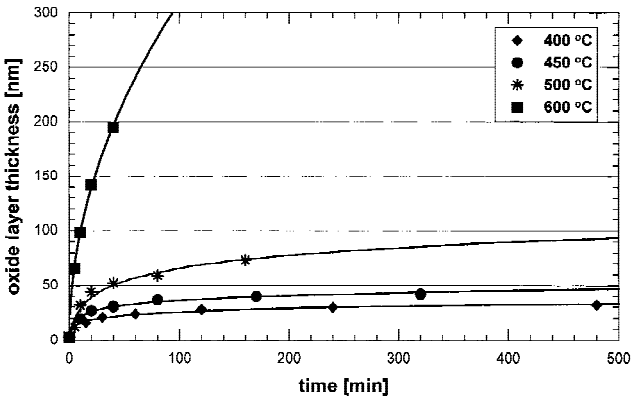

Figure 5. Thickness of oxide layers on cp-Ti after thermal oxidation as a function of temperature and time measured by means of ellipsometry.

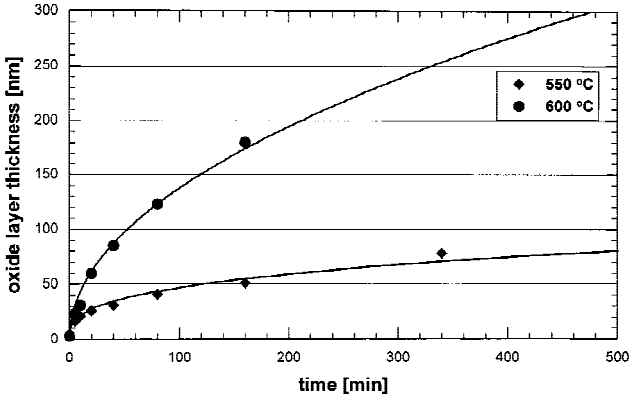

Figure 6. Thickness of oxide layers of Ti6A14V after thermal oxidation as a function of temperature and time measured by means of ellipsometry.

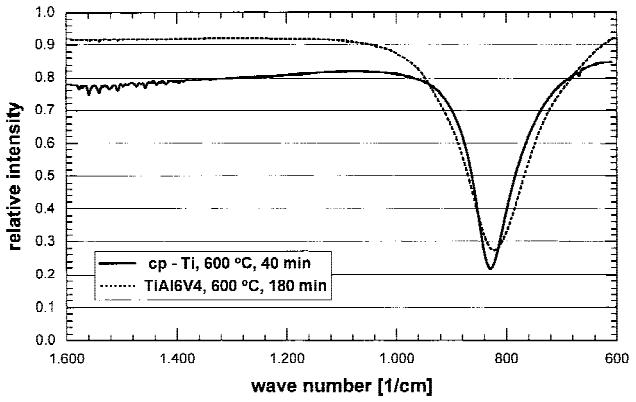

Figure 7. IR spectra of oxide layers of cp-Ti and Ti6A14V of almost equal thickness (190 nm) after thermal oxidation.

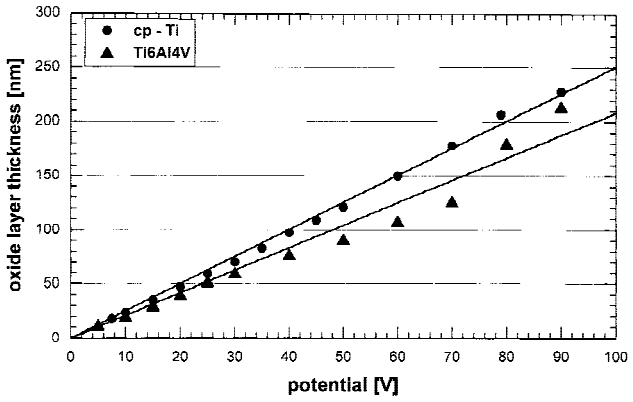

Figure 8. Oxide layer thickness after anodic oxidation as a function of the final potential.

For both, only one broad band occurs at around 830 cm^{-1}, indicating that the layers consist only of TiO_2 in the rutile structure.[20,21] In the literature it is reported that according to ESCA analysis thermal and anodic oxide films on Ti6Al4V have a small content of aluminium and vanadium oxide.[22,23] Bands for aluminium oxide, for example, Al_2O_3 at 960 cm^{-1},[24] or vanadium oxide, for example, V_2O_5 at 1040 cm^{-1},[25] were not observed. A reason for the missing bands of aluminium oxide and vanadium oxide might be the small spectral intensity due to a low content of these oxides in the films.

Coatings produced by means of the anodic oxidation

For cp-Ti, the applied constant current density was 5 mA/cm^2. Above a final potential of 50 V at this current density no further growth of the oxide layer is observed. This can be interpreted in terms of changes in the oxide structure from amorphous to crystalline during the growth of the film. The amorphous film at the beginning of the oxidation becomes more and more crystalline with progressive anodizing. As a result, there is a change from ionic conductivity, which is necessary for the film growth, to electronic conductivity, where the growth is retarded and finally stops.[26] By increasing the current density up to 10 mA/cm^2, higher final potentials can be reached before the growth stops and thus thicker films can be produced. For Ti6Al4V, a current density of 2 mA/cm^2 was sufficient for the whole range of potential up to 100 V. The aluminium and vanadium of the alloy seem to hinder the crystallization of TiO_2 in the film.

In Figure 8 the thickness of the anodic oxide films is plotted against the final potential. It can be seen that the thickness depends linearly on the applied voltage for cp-Ti and Ti6Al4V. The growth rates were determined to be 2.5 nm/V for cp-Ti and 2.1 nm/V for Ti6Al4V. The macroscopic surface topography of the anodized samples was much smoother than that of the thermally oxidized samples. The color of the samples, which depends on the thickness of the layers, is summarized in Table III.

The infrared spectra of the oxide layers after anodizing show a broad absorption in the wave number range from 600 to 1000 cm^{-1}, consisting of the superposition of several absorption bands (Fig. 9). A peak fit program was applied to the spectra, assuming the absorption bands to be of gaussian shape. For the use of the peak fit program, the spectra were mirrored on the baseline.

Ti–O bonds in TiO_4 tetrahedrons, which build up an amorphous structure like SiO_4 tetrahedrons in silica glass, show absorption around 770 and 940 cm^{-1}.[27,28] Ti–O bonds in crystalline TiO_2 in the anatase structure, which consists of TiO_6 octahedrons, absorb at about 870 cm^{-1} and in the range from 700 to 500 cm^{-1} (690, 590, 550 cm^{-1}).[29,30] For both materials, an amorphous TiO_2 layer with small amounts of crystalline anatase was formed at lower potentials. For the same current density, with increasing formation voltage more and more amorphous TiO_2 transforms into the crystalline anatase structure, i.e., TiO_4 tetrahedrons transform to TiO_6 octahedrons. The area of the fitted single absorption bands gives approximate informa-

TABLE III
Colors of Oxide Layers after Anodic Oxidation

Layer Thickness (nm)	10–25	25–40	40–50	50–80	80–120	120–150	150–180	180–210
Color	golden	purple	deep blue	light blue	yellow	orange	purple	green

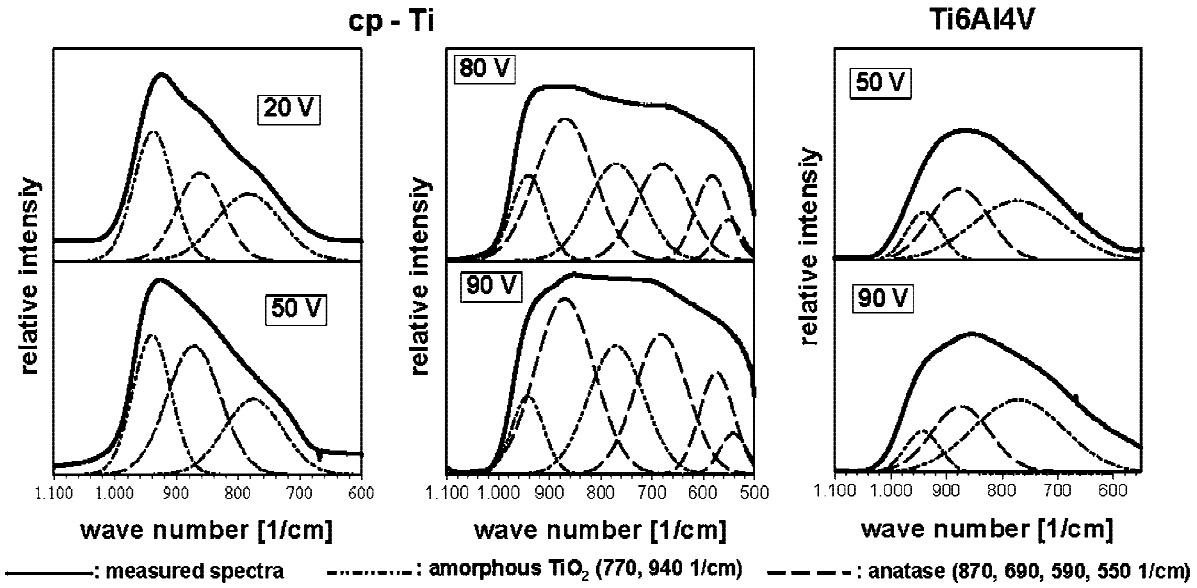

Figure 9. IR spectra and fitted single bands of samples, anodically oxidized for different final potentials.

tion on the amount of the different TiO_2 structures. The information cannot be exact because the spectral sensitivity coefficients may vary for the different bands. Unfortunatly, these coefficients are not known. With that restriction the amount of amorphous TiO_2 in the layer on cp-Ti decreases from approximately 70% for 20 V to 30% for 90 V final potential. For Ti6Al4V, the transformation takes place at higher final potentials. The amount of anatase for 90 V is only 30%, leading to the result, that the crystallization of the oxide on Ti6Al4V is hindered more than on cp-Ti.

Coatings produced by means of the sol-gel process

The determined thicknesses of the dried and the annealed films on Ti6Al4V as a function of the number of spins are plotted in Figure 10. The thickness of the films decreases during annealing, because of evaporating water and residual alcohols. The shrinkage is about 30% for the 1% sol and 20% for the 3% sol. The increase of the film thickness per spin is about 12 nm in the case of the 1% sol and 42 nm of the 3% sol. For samples coated once with the 1% sol, the oxide layer is thicker after annealing than after drying, because simultaneously with the shrinkage by evaporation of water and alcohol, the film thickness increases due to thermal oxidation at this annealing temperature. Under the same parameters cp-Ti showed a similar behavior.

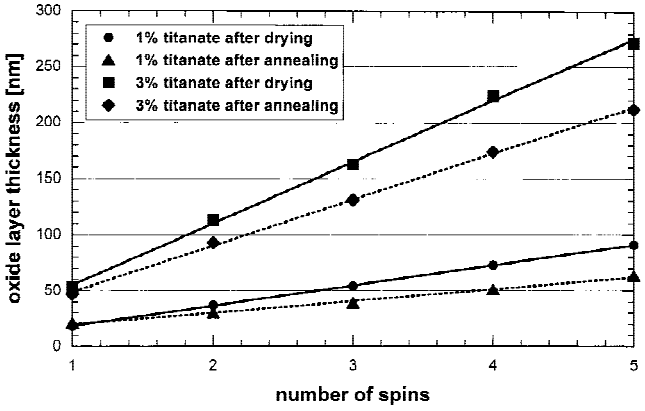

Figure 10. Thickness of oxide layers produced on Ti6A14V by the sol-gel process.

The IR measurements were carried out on samples of cp-Ti and Ti6Al4V spin coated four times with a sol containing 3% TBOT with a resulting thickness of about 170 nm after annealing at 350, 450, 550, and 650°C for 1 h. Because of the superposition of the peaks in the spectra, the position and the intensity of the absorption bands were determined by a peakfit program. Figure 11 shows the measured IR spectra and the fitted bands of the sol-gel derived films on cp-Ti and Ti6Al4V. The two bands at 770 and 940 cm^{-1} are associated with TiO_4 tetrahedrons that are formed by polycondensation of $Ti(OH)_4$ particles and are bonded by Ti–O–Ti bridges. At higher temperatures the TiO_4 tetrahedrons transform into TiO_6 octahedrons, building crystalline TiO_2. The bands corresponding to crystalline TiO_2 occur at about 830 cm^{-1} for the rutile structure and 870 cm^{-1} for the anatase structure. The phase composition of the sol-gel films is shown in Figure 12.

After drying, the oxide film consists of amorphous TiO_2 and anatase. The amount of amorphous TiO_2 decreases with increasing annealing temperature while the amount of anatase that is built up of transformed

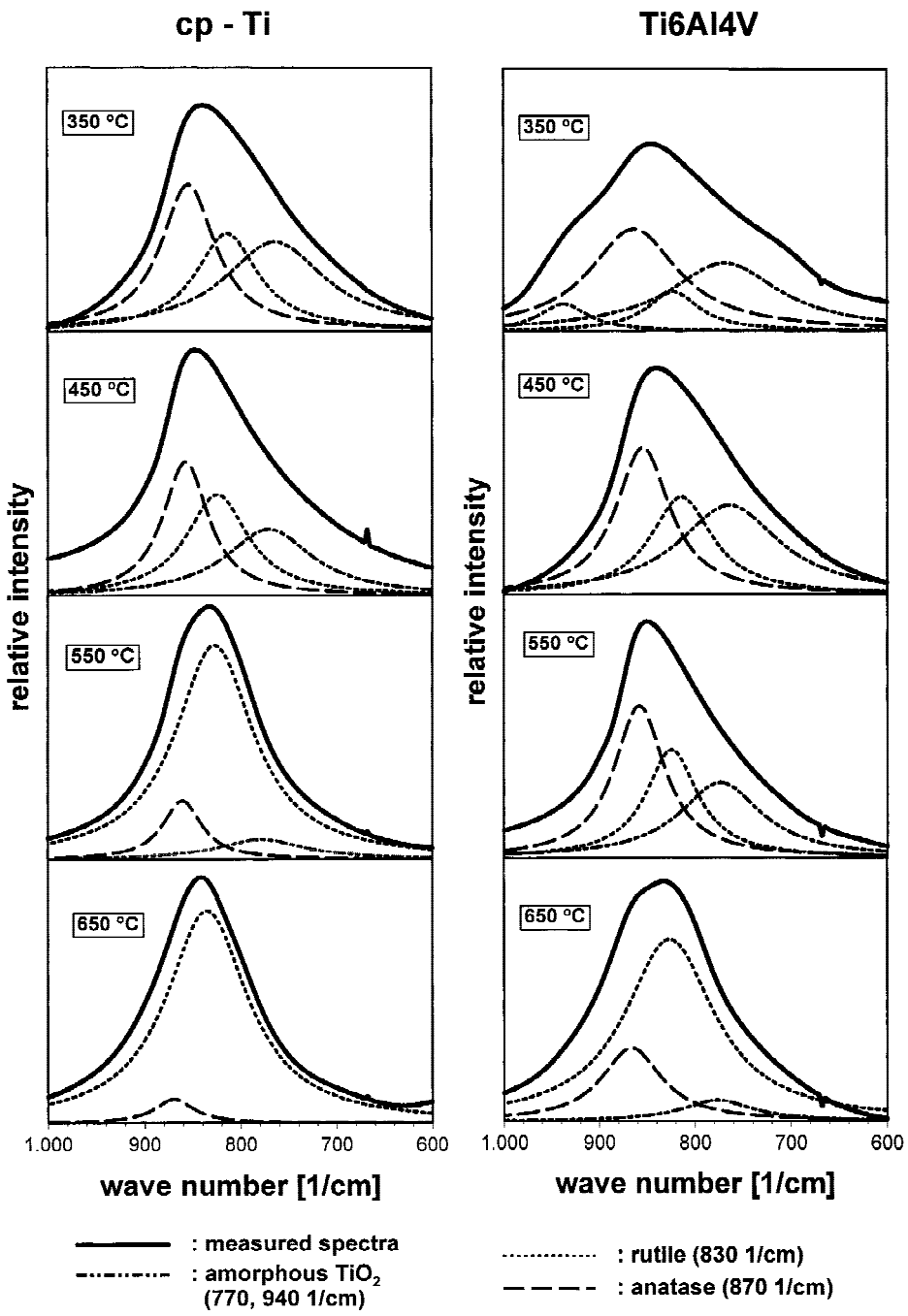

Figure 11. IR spectra and fitted single bands of sol-gel-coated samples of cp-Ti and of Ti6A14V annealed for 1 h at different temperatures.

amorphous TiO_2, is higher after firing at 350°C. At higher temperatures more and more anatase transforms into rutile which is also present at 350°C. The amount of rutile steadily increases up to 650°C where nearly the whole film consists of rutile.

The substrate material seems to have an influence on the kinetics of the transformation from amorphous to anatase and from anatase to rutile. After firing at 550°C, the sol-gel film on Ti6Al4V consists of 35% anatase. In contrast, after the same heat treatment of the film on cp-Ti only 10% anatase is determined. The transformation of the oxide layers from anatase to rutile on Ti6Al4V starts at temperatures 100°C higher compared to cp-Ti. The influence on the transformation may be allocated to the grain size of the substrate material or to alloying elements, which diffuse into the film during heat treatment and may stabilize different TiO_2 structures.[31]

To confirm the results of the coated materials, TiO_2 powder was produced by evaporating sol containing 3% TBOT. This powder was annealed at 450, 500, 550, 650, and 750°C for 1 h in a laboratory furnace in air.

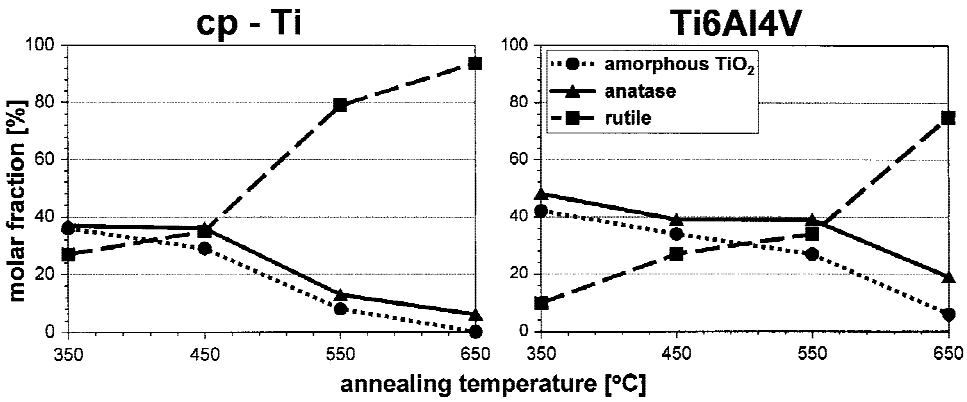

Figure 12. Phase composition of the sol-gel oxide layers after annealing at different temperatures for 1 h.

The phase composition of the powder samples was determined by X-ray diffractometry. The results are shown in Figure 13. In the dried powder no crystalline phase was detected. Thus, an amorphous structure is assumed. After annealing at 450°C only one crystalline phase, anatase, was detected. At 500°C anatase is still the prevailing phase, but a small rutile peak can be observed. With increasing temperature the transformation from anatase to rutile proceeds until pure rutile is present at 750°C.

In comparison to the oxide films, the phase transitions of the powder samples from amorphous to anatase and from anatase to rutile are shifted to higher temperatures for the same annealing time. This can be explained by the heterogeneous nucleation of the TiO_2 crystallites on the surface of the substrate material. By contrast, the nucleation in the powder is more homogenous and thus occurs at higher temperatures.[11] Another reason might be the size of the crystallites after nucleation, which is in the nanometer region. Because of the small size there is a strong broadening of the X-ray reflexes, and they are superimposed by the scattering background. At higher annealing temperatures the crystallites grow and obtain sizes at which the diffraction peaks are visible. As IR spectroscopy uses the absorption of bonds, in contrast to X-ray diffractometry, small crystallites can be detected.

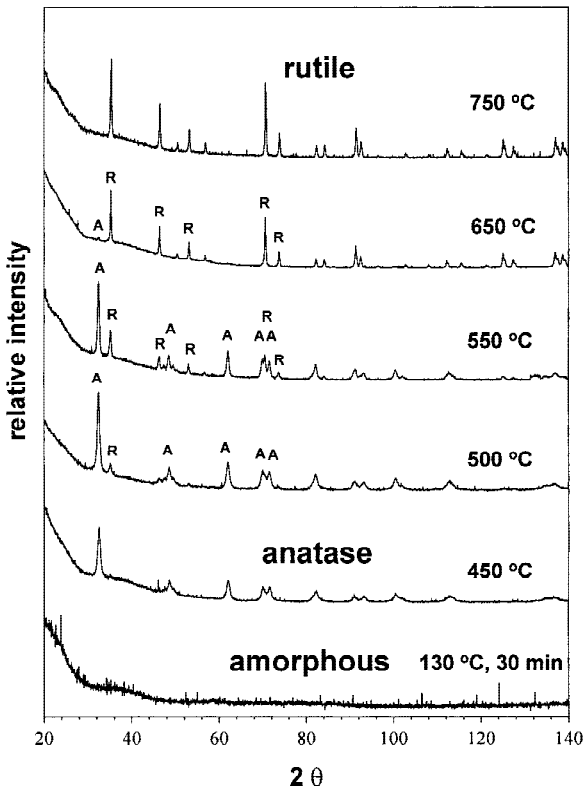

Figure 13. Phase composition of sol-gel powder samples after heat treatment at different temperatures for 1 h.

Results of the corrosion tests

Figure 14 shows the current density–potential curves of oxidized, coated, and polished cp-Ti and Ti6Al4V samples with a scan rate of 0.5 mV/s. For all samples, the range of passivity with a current density below 10 $\mu A/cm^2$ extends from 0 to 1800 mV. Above 1800 mV the current density increases for all samples. The anodically oxidized samples show the smallest and the thermally oxidized samples the largest increase.

For a more precise determination of the passive current density measurements in the potential range from −500 to 1200 mV, with a scan rate of 0.1 mV/s were performed. The curves for cp-Ti and Ti6Al4V are shown in Figure 15. In all cases, the current densities in the range of the body potential (400–500 mV) are below 1 $\mu A/cm^2$. The measured data shows a variance of 0.2 to 0.5%, because of the tolerance of the used galvano- and potentiostates.

Table IV shows the measured passive current densities. It can be seen that the oxidized and coated samples have a current density in the passive range

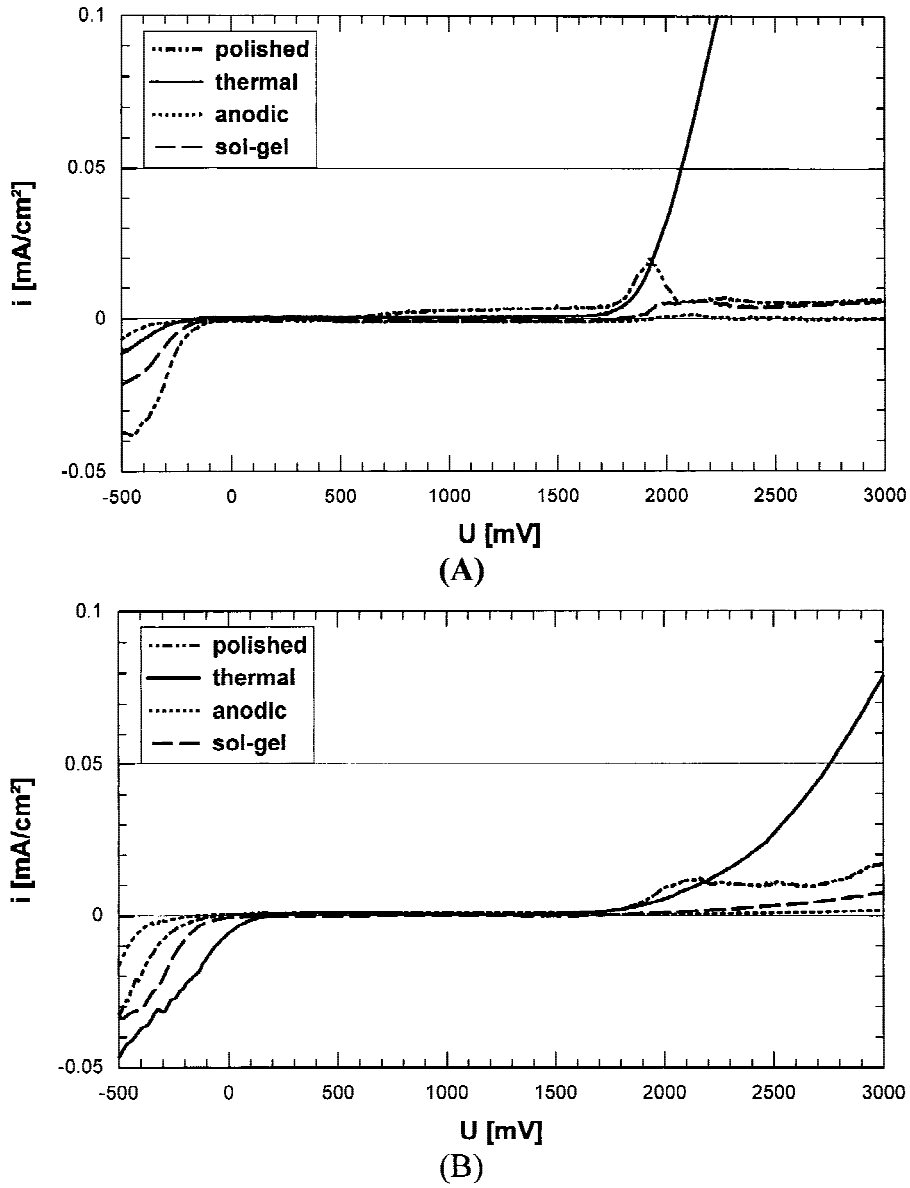

Figure 14. Current density–potential curves of oxidized and coated samples of cp-Ti (A) and Ti6A14V (B) at a scan rate of 0.5 mV/s.

that is much lower than that of the polished samples which have a thinner, "natural" oxide layer. For cp-Ti, the anodic oxidized samples show the lowest passive current density, while for Ti6Al4V the thermal oxidized and the sol-gel samples have the lowest current density in the passive range. The polished sample of Ti6Al4V shows a higher passive current density than that of cp-Ti. As a result, the corrosion resistance of cp-Ti and Ti6Al4V can be improved by thickening the oxide film.

CONCLUSION

Titanium-based alloys have found widespread use as implant materials. The reason for their high biocompatibility is the titanium oxide layer TiO_2 on its surface.

On cp-Ti and Ti6Al4V, as substrate materials, oxide layers were produced by thermal oxidation, anodic oxidation and by the sol-gel process. The thickness, the structure, and the phases of these oxide layers were determined.

For thermal oxidation, the thickness of the oxide films shows a logarithmic or a parabolic growth rate, respectively, depending on the annealing temperature. The oxide layer always consists of TiO_2 in the rutile structure. Aluminium or vanadium oxide in the films on Ti6Al4V could not be detected by IR spectroscopy. This problem can be solved by additional XPS and AES experiments.

The thickness of the anodic films corresponds lin-

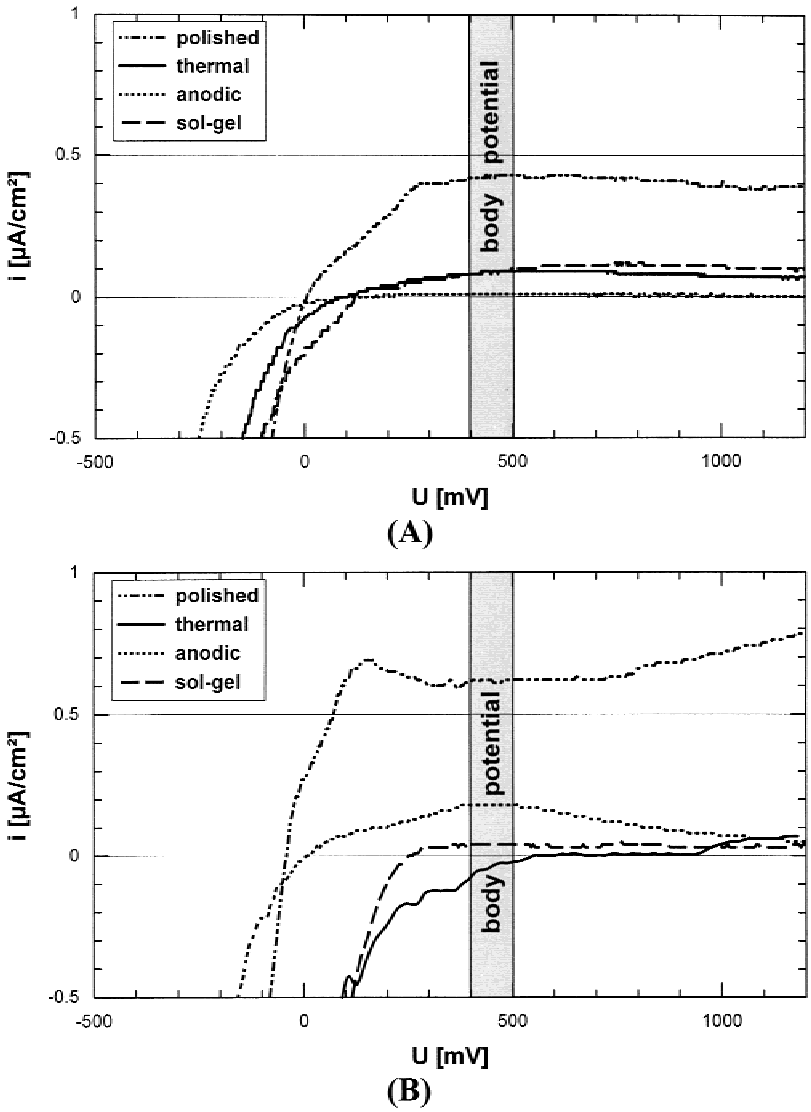

Figure 15. Current density–potential curves of polished, oxidized, and coated samples of cp-Ti (A) and Ti6A14V (B) at a scan rate of 0.1 mV/s.

early to the finally applied potential of the galvanostatic anodization. The TiO_2 layer is a mixture of amorphous and anatase structure. The amounts of anatase increase with increasing final potential. On Ti6Al4V, the transition from amorphous material to anatase starts at higher potentials.

By repetition of the coating procedure the thickness of the sol-gel films can be varied in steps of 12 nm for 1% TBOT solution and 40 nm for 3% TBOT solution. The structure of the TiO_2 sol-gel film is sucessively amorphous, anatase, and rutile with increasing temperature of the heat treatment. Higher temperatures accelerate the transitions from amorphous to anatase and from anatase to rutile.

In comparison with the polished samples, the corrosion resistance of cp-Ti and Ti6Al4V is enhanced by an oxide layer thickness of 100 nm, independent on the oxidation procedure. The polished samples of cp-Ti show a lower current density than that of Ti6Al4V in the same condition. The potential of passivity for all samples ranges from 0 to 1800 mV with current densities between 0 and 0.62 $\mu A/cm^2$.

TABLE IV
Passive Current Densities of Samples of cp-Ti and Ti6A14V with Different Oxide Layers

Substrate Material	Oxide Layer	Passive Current Density ($\mu A/cm^2$)
cp-Ti	polished (natural oxide layer)	0.39
cp-Ti	thermal oxidation	0.07
cp-Ti	anodic oxidation	0.00
cp-Ti	sol-gel process	0.09
Ti6A14V	polished (natural oxide layer)	0.62
Ti6A14V	thermal oxidation	0.08
Ti6A14V	anodic oxidation	0.05
Ti6A14V	sol-gel process	0.03

References

1. Helsen JA, Breme HJ. Metals as Biomaterials. Chichester: John Wiley & Sons; 1998.
2. Long M, Rack HJ. Review—Titanium alloys in total joint replacement—A materials science perspective. Biomaterials 1998;19:1621–1639.
3. Worch H, Scharnweber D. Biologisierte Titanwerkstoffe. Z Metallk 1998;89(2):153–163.
4. Wadewitz V, Breme J. TiTa-Legierungen für dentale Implantate—Korrosionsverhalten, einschließlich Kontaktkorrosion. Z Zahnärztl Implant 1989;5(2):116–120.
5. Dislich H, Hussmann E. Amorphous and crystalline dip coatings obtained from organometallic solutions: Procedures, chemical processes and products. Thin Solid Films 1981;77: 129–139.
6. Holleman AF, Wiberg E. Lehrbuch der anorganische Chemie. Berlin: Walter de Gruyter; 1976.
7. Fukushima K, Yamada I, Takagi T. Charakteristics of TiO_2 films deposited by a reactive ionized cluster beam. J Appl Phys 1985;58(2):4146–4149.
8. Cox JD. Key values for thermodynamics. New York: Hemisphere Publishing Co.; 1989.
9. Wagman D. Reference data. J Phys Chem 1982;Suppl 2.
10. Chase M. Thermochemical tables, 3rd ed. J Phys Chem 1985; 14:Suppl 1.
11. Byun C, Jang JW, Kim IT, Hong KS, Lee BW. Anatase-to-rutile transition of titania thin films prepared by MOCVD. Mater Res Bull 1997;32(4):431–440.
12. Kilpadi DV, Lemmons JE. The effect of surface and heat treatment on corrosion of unalloyed titanium implants. 16th South Biomed Eng Conf, Biloxi, MS, April 1997.
13. Xie SF. Corrosion behaviour of titanium anodic oxide films. Key Eng Mater 1988;20–28(1):397–402.
14. Samuneva B, Kozhukharov V, Trapalis C. Sol-gel processing of titanium-containing thin coatings. J Mater Sci 1993;28:2353–2360.
15. Hu L, Yoko T, Kozuka H, Sakka S. Effects of solvent on properties of sol-gel-derived TiO_2 coating films. Thin Solid Films 1992;219:18–23.
16. Heidenau F, Schmidt H, Stenzel F, Ziegler G. Herstellung von Titanoxidschichten mit variabler Porengröße über Sol-Gel-Synthesen. In: Dimigen H, Paatsch W, editors. Proceedings "Werkstoffwoche 1998." Bd 9, Symposium 11: Oberflächentechnik.
17. Rausch N, Burte EP. Thin TiO_2 films prepared by low pressure chemical vapor deposition. J Electrochem Soc 1993;140(1):145–149.
18. Tabellion J. Numerische und experimentelle Eigenspannungsanalyse atmosphärisch plasmagespritzter Al_2O_3-Schichten auf Metall- und Glassubstraten. Diplomarbeit, Saarbrücken; 1998.
19. Anders S, Anders A, Rubin M, Wang Z, Raoux S, Kong F, Brown I. Formation of metal oxides by cathodic arc deposition. Surface Coat Technol 1995;76(1–3):167–173.
20. Phillippi CM, Lyon SR. Longitudinal-optical phonons in TiO_2 (rutile) thin-film spectra. Phys Rev B3 1971;6:2086–2087.
21. Thibault S. Infrared reflection-absorption spectra of oxide films on titanium. Thin Solid Films 1976;35:L33–L35.
22. Hazan R, Brener R, Oron U. Bone growth to metal implants is regulated by their surface properties. Biomaterials 1993;8:570–574.
23. Ask M, Lausmaa J, Kasemo B. Preparation and surface spectroscopic characterization of oxide films on TiAl6V4. Appl Surf Sci 1988–1989;35:283–301.
24. Khafagy AH, Ewaida MA, Higazy AA, Ghoneim MMS, Hager IZ, El-Bahnasawy R. Infrared spectra and composition dependence investigations of the vitreous V_2O_5/P_2O_5 system. J Mater Sci 1992;27(6):1435–1439.
25. Maeland AJ, Rittenhouse R, Lahar W, Romano PV. Infrared reflection-absorption spectra of anodic oxide films on aluminium. Thin Solid Films 1974;21:67–72.
26. Leach JSL, Sidgwick DH. Anodic oxidation of titanium. 8th International congress on Metallic Corrosion, Mainz, Proceedings, pp. 82–86.
27. Morsi MM, El-Shennawi AWA. Some physical properties of silicate glasses containing TiO_2 in relation to their structure. Phys Chem Glas 1984;25(3):64–68.
28. Nakamoto K. Infrared and raman spectra of inorganic and coordination compounds. New York: John Wiley & Sons; 1986.
29. Gonzales RJ, Zallen R. Optical studies of nanophase titania. NATO ASI Series 1997;23:395–403.
30. Villegas MA, de Pablos A, Ferrnádez Navarro JM. Structural and microstructural study of glasses in the $LiO–TiO_2–SiO_2$ system. J Mater Sci 1995;30:995–999.
31. Reddy BM, Ganesh I, Reddy VR. Influence of V_20_5 and Nb_2O_5 on thermal stability of TiO_2-anatase. J Mater Sci Lett 1998;17(22):1913–1915.